applied sciences

MDPI

Article

H_2 Optimization of a New Type of Tuned Lever Inerter-like Mass Damper (TLIMD) for Attenuating Structure Vibrations

Kai Xu [1], Weiwei Wang [1], Hui Liang [1], Aifeng Liu [1], Jianmin Yang [1], Jingzhou Gao [1] and Bei Chen [2,3,*]

[1] Northwest Institute of Mechanical & Electrical Engineering, Xianyang 712099, China; xukai0525@126.com (K.X.); 18406595653@163.com (W.W.); drywet@163.com (H.L.); avonliu0331023@163.com (A.L.); jimyuang@sohu.com (J.Y.); fengniao8691@163.com (J.G.)
[2] National Key Laboratory of Bridge Engineering Safety and Resilience, Hunan University, Changsha 410082, China
[3] Key Laboratory for Wind and Bridge Engineering, Hunan University, Changsha 410082, China
* Correspondence: chamber@hnu.edu.cn

Abstract: The lever or the lever-type mechanism can achieve an inertia amplification effect by appropriately calibrating its structural configuration, and it is also proven to be one of the most cost-effective solution for the inerter realization compared with other mechanical devices. Benefitting from this property, the present paper adopted a new type of tuned lever inerter-like mass damper (TLIMD) for attenuating stochastic load-induced structure dynamic responses. A set of closed-form formulae for the TLIMD optimal parameters are developed by the use of H_2 norm optimization criterion, wherein the structure's inherent damping is explicitly accounted for. It is theoretically demonstrated that the TLIMD optimal parameters are mainly dominated by three critical parameters, i.e., the damper mass ratio, the lever length ratio (known as the inertia amplification ratio) and also the host structural damping. The proposed formulae for the TLIMD optimization are validated through the seismic analysis, where two classic inerter-based dampers (i.e., the tuned mass damper inerter (TMDI) and the tuned inerter damper (TID)) optimized by the numerical technique are included in the discussion. It is found that the TLIMD has a superior advantage in reducing the structure responses and also exhibits stronger robustness for the detuning condition than the classic inerter-based dampers. Furthermore, the increase in the damper mass ratio and the lever length ratio can be beneficial for enhancing its performance.

Keywords: tuned lever inerter-like mass damper; dual-equivalent linearization; H_2 normal optimization; vibration control; seismic response

check for updates

Citation: Xu, K.; Wang, W.; Liang, H.; Liu, A.; Yang, J.; Gao, J.; Chen, B. H_2 Optimization of a New Type of Tuned Lever Inerter-like Mass Damper (TLIMD) for Attenuating Structure Vibrations. *Appl. Sci.* **2024**, *14*, 10059. https://doi.org/10.3390/app142110059

Academic Editors: Rosario Pecora and Junhong Park

Received: 10 July 2024
Revised: 17 September 2024
Accepted: 17 October 2024
Published: 4 November 2024

Copyright: © 2024 by the authors. Licensee MDPI, Basel, Switzerland. This article is an open access article distributed under the terms and conditions of the Creative Commons Attribution (CC BY) license (https://creativecommons.org/licenses/by/4.0/).

1. Introduction

The inerter is known as a powerful device to amplify the inertial effect without significantly increasing the physical mass [1–3]. Benefiting from this favourable feature, the inerter has been widely utilized in the conventional damping devices (both dynamic vibration absorber and energy dissipator) for enhancing their performance. Typical inerter-based dampers include the tuned mass damper inerter (TMDI) [4–6], the tuned inerter damper (TID) [7–9], the viscous inertial mass damper (VIMD) [10–12] and even the inerter-based active or semi-active dampers [13–15]. Another important consideration is the physical realization, and it primarily includes mechanisms such as ball-screw, rack-and-pinion, hydraulic, etc. [16–19]. However, almost all these conventional inerter mechanical devices need specialized manufacturing equipment, and thus create extra costs for the damper utilization. Fortunately, the lever mechanism, as one of the most traditional and simple mechanical devices, also has similar inertial amplification characteristics [20]. Although the end point of the lever arm and the fulcrum, as the two terminals, does not strictly meet the definition of the ideal inerter due to its nonnegligible nonlinear effect [21–23], the lever is still considered to be one of the most cost-effective inertial amplification mechanisms.

Many scholars have performed various studies on lever dampers, and the results show that they have good control performance. Flamnelly et al. [24] conducted the pioneering work regarding the lever-type damper. A so-called dynamic anti-resonance vibration isolator (DAVI) was introduced into the base-isolation system and achieved excellent control performance. Since then, the lever-type damper has attracted a great attention. It is interesting to point out that the DAVI was initially utilized in the field of helicopter research to prevent undesirable vibrations of the cabin caused by the engine vibration. Li et al. [20] conceived three new types of lever-type DAVIs (different combinations of the lever and the conventional spring and dashpot). It was shown that the lever mechanism can enhance the performance of the conventional vibration isolation system. Jing et al. [25,26] introduced this lever mechanism into an X-shape structure for achieving broadband isolation system. Zang et al. [27] conceived a novel lever-type based on a nonlinear damper, which incorporated the nonlinear energy sink with the lever mechanism. It was theoretically demonstrated that the lever mechanism can improve the damping performance of the original nonlinear energy sink. Similar work has been conducted by Yang et al. [28], who embedded a lever into a bistable nonlinear energy sink, whose results indicated that the lever can improve energy harvesting performance. For further improvement of the lever-type dampers, an additional lever or even multiple levers may be an effective solution. Yilmaz et al. [29] developed two lever-type vibration isolators given the practical arrangement configuration, and it was shown that a smaller damping is more beneficial for achieving broadband isolation. In their following study [30], more complicated two levers vibration isolators are proposed; the results showed that such design can achieve a lower band frequency. Yan et al. [31–34] included a lever into the eddy current-based dampers, which significantly enhanced the original damper performance.

In addition to the foundation vibration isolation system, the lever mechanism also has a good application prospect in the field of the dynamic vibration absorber (DVA). Li et al. [35] conceived novel lever-type devices called the lever-arm tuned mass damper inerter (LTMDI), where an inerter was implemented to enhance the lever-type performance. Gu et al. [36] conducted the first investigation, where the lever arm is embedded into the conventional tuned mass damper (LTMD). However, a detailed theoretical investigation was not performed in their work. Lee et al. [37] made a further effort. It was found that the LTMD is superior to the conventional TMD in terms of the spring static stretch and the optimal damping requirement. This feature makes the LTMD more favourable to engineers. Li et al. [38] conceived a new type of LTMD, where two concentrated masses are attached to the lever two endpoints. Likewise, this new device exhibits better control performance than the conventional TMD. In addition to the one LTMD configuration, a multiple LTMDs configuration strategy was also adopted by many researchers [39]. In addition to those passive damping devices, the lever mechanism is also introduced into the active or semi-active dampers and achieved excellent performance. Li et al. [13,14,40] included this lever mechanism into active dampers. The results show that the lever enhanced active damper can significantly improve the damping performance for the ground motion-excited structure response. Gu et al. [15] developed a novel lever-based semi-active damper, in which a movable concentrated mass is employed and achieved desirable results.

The mentioned investigations implies that this classic lever mechanism can enhance the performance of the original dampers using an appropriate design. In consideration of this promising result, a novel tuned lever inerter-like mass damper (TLIMD) was developed in our previous study [22], and its nonlinear dynamic properties (i.e., the large-angle situation) under a harmonic excitation were systematically discussed. However, the TLIMD optimization scheme and its control performance assessment under practical conditions (i.e., the small-angle situation, the structural inherent damping and also the stochastic load-induced structure vibrations) are still lacking. To remedy this issue, a set of closed-form formulae for the TLIMD optimal design is developed (using the classic H_2 norm optimization) in the present study under the stochastic load-induced structure vibration condition. The structural inherent damping contribution is accounted for by adopting a

simplification procedure for the primary damped system. Thus, more generalized formulae for the TLIMD optimization are developed. Three critical parameters (including the damper mass ratio, the lever length ratio and the host structural damping) that dominate the TLIMD optimal performance are revealed from a theoretical perspective. The accuracy of the proposed formulae is verified by the comparison results with the ones obtained by the numerical optimization technique (here using the particle swarm optimization). The seismic analysis is conducted to evaluate its control performance and robustness property. The results show the optimized TLIMD (by the proposed formulae) is significantly superior compared to conventional inerter-based dampers.

2. The SDOF System with a Grounded TLIMD

In general terms, a structure equipped with a grounded tuned lever inerter-like mass damper (TLIMD, first introduced in [22]) can be represented by an analogue TLIMD with a single-degree-of-freedom (SDOF) system (TLIMD-SDOF, shown in Figure 1a), with the DOF corresponding to the target mode, normally the fundamental mode of the primary structure, for the damper design. The m_1, k_1 and c_1 are the mass, stiffness and damping coefficients of the host structure, respectively. The TLIMD comprises a rigid lever, having an auxiliary concentrated mass m_2 (located at point P_e) and a parallel dashpot (c_2)–spring (k_2) element with its terminals attached to the host structure and the lever (at point P_r), respectively, as shown in Figure 1b. The total mass of the lever is $m_3 = \rho L$, where ρ and L denote the mass per unit length and the overall lever length, respectively. Two Cartesian coordinate systems are introduced for the description of this coupled system. The (x,y)-coordinate system denotes the global fixed coordinate system, with the original point 'O' located at the centre of the fulcrum P_s. The (x',y')-coordinate system denotes the local rotating coordinate system fixed to the lever, with the original point coinciding with 'O'.

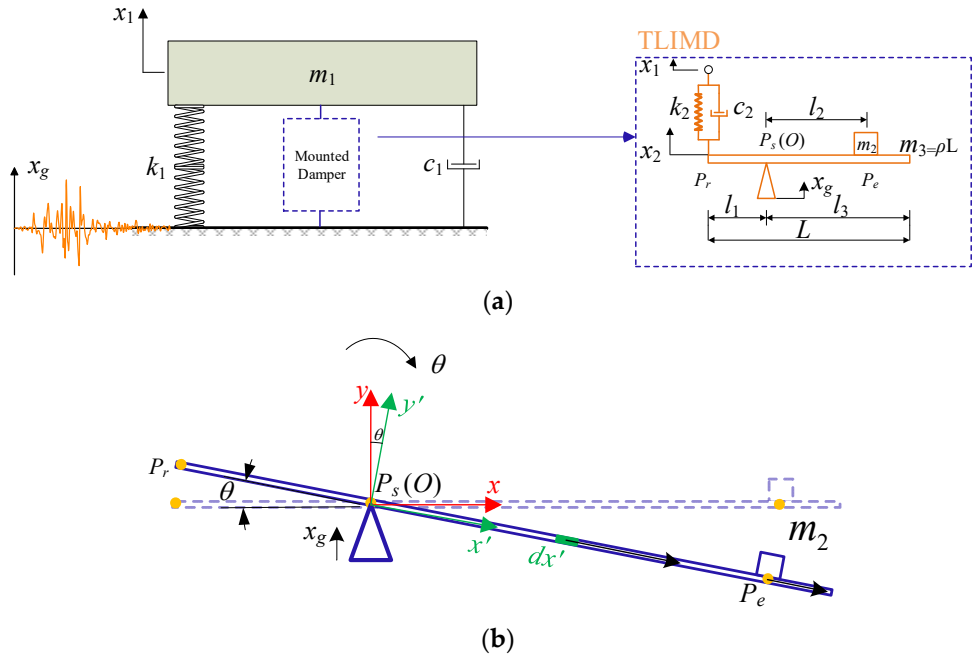


Figure 1. (**a**) The analogue TLIMD-SDOF system. (**b**) Schematic configuration of the lever.

In Figure 1, the rotating angle of the lever, denoted as θ, is defined with a positive value representing clockwise rotation. The location of points P_r, P_e and the lever right-side end point with respect to the fulcrum P_s in the rotating coordinate system are identified by l_1, l_2 and l_3, respectively. Note that $L = l_1 + l_3$. The ground motion is denoted by x_g, and the relative displacement responses (with respect to. the ground) of the host structure and the lever (at point P_r) are denoted by x_1 and x_2, respectively.

2.1. Equations of Motion (EOMs)

In terms of the two coordinates and motion parameters defined in the primary analogue TLIMD-SDOF system, as shown in Figure 1, the kinetic energy T, the potential energy V and the dissipation function D of this coupled system can be obtained:

$$\begin{aligned} T &= \frac{1}{2}m_1\left(\dot{x}_1+\dot{x}_g\right)^2+\frac{1}{2}m_2[\left(-\dot{\theta}l_2\cos\theta+\dot{x}_g\right)^2+\left(-\dot{\theta}l_2\sin\theta\right)^2] \\ &\quad +\frac{1}{2}\int_{-l_1}^{l_3}\rho[\left(-\dot{\theta}x\prime\cos\theta+\dot{x}_g\right)^2+\left(-\dot{\theta}x\prime\sin\theta\right)^2]dx\prime \\ V &= \frac{1}{2}k_1x_1^2+\frac{1}{2}k_2(x_1-l_1\sin\theta)^2 \\ D &= \frac{1}{2}c_1\dot{x}_1^2+\frac{1}{2}c_2\left(\dot{x}_1-\dot{\theta}l_1\cos\theta\right)^2 \end{aligned} \tag{1}$$

Thus, the original nonlinear EOMs for the primary analogue TLIMD-SDOF system can be developed using the Lagrangian equation,

$$\begin{aligned} &m_1\ddot{x}_1+k_1x_1+k_2(x_1-l_1\sin\theta)+c_1\dot{x}_1+c_2(\dot{x}_1-\dot{\theta}l_1\cos\theta)=-m_1\ddot{x}_g \\ &[m_2{l_2}^2+\tfrac{1}{3}m_3({l_3}^2-l_1l_3+{l_1}^2)]\ddot{\theta}-k_2(x_1-l_1\sin\theta)(l_1\cos\theta)-c_2(\dot{x}_1-\dot{\theta}l_1\cos\theta)(l_1\cos\theta) \\ &=\ddot{x}_g\cos\theta[m_2l_2+\tfrac{1}{2}m_3(l_3-l_1)] \end{aligned} \tag{2}$$

For the development of closed-form formulae for the TLIMD optimal parameters, the small-angle approximation that is commonly utilized in the lever-type damper design [31,41] is imposed. The large-angle situation, which may introduce some nonlinear coupling terms, is investigated in our previous work, cf. [22]. The linearized EOM for this coupled system yields the following expressions:

$$\begin{aligned} &m_1\ddot{x}_1+k_1x_1+k_2(x_1-x_2)+c_2(\dot{x}_1-\dot{x}_2)=-m_1\ddot{x}_g \\ &[m_2{\alpha_1}^2+\tfrac{1}{3}m_3({\alpha_2}^2-\alpha_2+1)]\ddot{x}_2+k_2(x_2-x_1)+c_2(\dot{x}_2-\dot{x}_1)=\alpha_1m_2\ddot{x}_g+\tfrac{1}{2}m_3(\alpha_2-1)\ddot{x}_g \end{aligned} \tag{3}$$

where, $\alpha_1 = l_2/l_1$ and $\alpha_2 = l_3/l_1$ are the length ratios, which are crucial to the TLIMD performance, as demonstrated in the following sections. In practical applications, where the maximal inertial force is always desired, these two length ratios are commonly set to the same value (i.e., $\alpha_1 = \alpha_2 = \alpha$).

2.2. Harmonic Response Analysis

Assume a harmonic ground motion $\ddot{x}_g = a_{g0}e^{i\omega t}$ with an acceleration amplitude a_{g0} and an excitation frequency ω. i is the imaginary unit. The steady-state responses of the host structure and the lever (at point P_r) hold the following expressions:

$$x_1 = x_{10}e^{i\omega t},\ x_2 = x_{20}e^{i\omega t} \tag{4}$$

where the complex response amplitudes denoted by x_{10} and x_{20}.

A few non-dimensional parameters, including the mass ratio μ of the concentrated mass m_2 to the host structure m_1, the mass ratio μ_{32} of the lever mass m_3 to the concentrated mass m_2, the frequency ratio β of the host structure to the TLIMD, and the damping ratios (ζ_1 and ζ_2) of both the host structure and the TLIMD, are introduced for the convenience of expression. ω_1 and ω_2 denote the natural frequencies of the primary structure and of the TLIMD, respectively. The excitation frequency ω and the time t are non-dimensional parameters as well, which are defined as

$$\mu=\frac{m_2}{m_1},\ \mu_{32}=\frac{m_3}{m_2},\ \omega_1=\sqrt{\frac{k_1}{m_1}},\ \omega_2=\sqrt{\frac{k_2}{m_2}},\ \beta=\frac{\omega_2}{\omega_1},\ \zeta_1=\frac{c_1}{2m_1\omega_1},\ \zeta_2=\frac{c_2}{2m_2\omega_2},\ \phi=\frac{\omega}{\omega_1},\ \tau=\omega_1t \tag{5}$$

Thus, (3) can be recast in a non-dimensional format, given as

$$\begin{aligned} &\ddot{z}_1+z_1+2\zeta_1\dot{z}_1+\mu\beta^2(z_1-z_2)+2\zeta_2\mu\beta(\dot{z}_1-\dot{z}_2)=-e^{i\phi\tau} \\ &[{\alpha_1}^2+\tfrac{1}{3}u_{32}(1-\alpha_2+{\alpha_2}^2)]\ddot{z}_2+\beta^2(z_2-z_1)+2\zeta_2\beta(\dot{z}_2-\dot{z}_1)=\alpha_1e^{i\phi\tau}+\tfrac{1}{2}u_{32}(\alpha_2-1)e^{i\phi\tau} \end{aligned} \tag{6}$$

where $z_1 = x_1\omega_1^2/a_{g0}$ and $z_2 = x_2\omega_1^2/a_{g0}$ represent the non-dimensional responses of the host structure and the end point (at point P_r) of the lever arm, respectively.

3. Optimal Calibration of the TLIMD

Theoretical calibration framework for the damper is commonly developed by adopting the un-damped structure assumption, where the structural inherent damping influence (on the damper optimization) is totally ignored. To remedy this drawback, Anh et al. [42] proposed a novel equivalent-linearization-based damper optimization procedure (for the classic TMD). They demonstrated that the damping c_1 and stiffness k_1 elements of the SDOF system (representing the primary system) can be approximately presented by an equivalent stiffness term k_{1e}, thereby resulting in an approximate un-damped SDOF system. Hence, the structural damping influence can be automatically included in their damper calibration process. To achieve better results, an updated dual-equivalent linearization method was developed in his follow-up research [42–44], which is also utilized in the present study. By the use of such an approximate system (i.e., the approximate un-damped SDOF system, shown in Figure 2), analytic solutions for the TLIMD optimal parameters (under the idealized case of white noise external excitation condition) is developed via the classic H_2 norm optimization criterion.

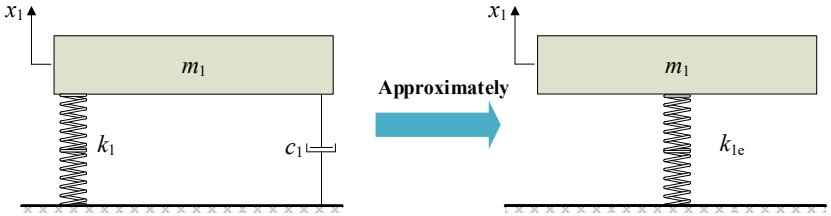


Figure 2. The approximate un-damped SDOF system.

3.1. Dual-Equivalent Linearization for the Primary Damped SDOF System

The original EOM for the primary damped SDOF system (shown in Figure 1a) can be written as

$$\ddot{x}_1 + {\omega_1}^2 x_1 + 2\zeta_1 \omega_1 \dot{x}_1 = 0 \tag{7}$$

where ω_1 and ζ_1 denote the natural frequency and damping ratio (defined in (5)), respectively.

The EOM for the approximate un-damped SDOF system (shown in Figure 2) can be constructed as

$$\ddot{x}_1 + {\omega_{1e}}^2 x_1 = 0 \tag{8}$$

where ${\omega_{1e}}^2 = k_{1e}/m_1 = \gamma + {\omega_1}^2$ is the natural frequency squared of the approximate un-damped SDOF system. The parameter γ indicates the contribution from the structural damping (of the primary damped SDOF system) to the equivalent stiffness term k_{1e} (of the approximate un-damped SDOF system), and it shall be determined by the following criterion [42].

$$P = \frac{1}{T}\int_0^T [(2\zeta_1\omega_1\dot{x}_1 - \gamma x_1)^2 + (\gamma x_1 - 2\lambda\zeta_1\omega_1\dot{x}_1)^2]dt \tag{9}$$

where T is a random period and λ is the so-called dual parameter. The coefficients γ and λ can be determined by

$$\frac{\partial P}{\partial \gamma} = 0, \ \frac{\partial P}{\partial \lambda} = 0 \tag{10}$$

where (∂/∂) denotes the partial derivative operator.

By inserting (9) into (10), a set of equations in terms of γ and λ can be developed:

$$\begin{array}{l} \gamma\int_0^T {x_1}^2 dt - (\lambda+1)\int_0^T \zeta_1\omega_1 x_1\dot{x}_1 dt = 0 \\ 2\lambda\int_0^T \zeta_1\omega_1 {\dot{x}_1}^2 dt - \gamma\int_0^T x_1\dot{x}_1 dt = 0 \end{array} \tag{11}$$

The above equations lead to the solutions for γ and λ, given as

$$\begin{aligned}\gamma &= 2\zeta_1\omega_1\frac{\int_0^T x_1\dot{x}_1dt}{\int_0^T {x_1}^2dt}\frac{\int_0^T {x_1}^2dt\int_0^T {\dot{x}_1}^2dt}{2\int_0^T {x_1}^2dt\int_0^T {\dot{x}_1}^2dt-(\int_0^T x_1\dot{x}_1dt)^2}\\ \lambda &= \frac{(\int_0^T x_1\dot{x}_1dt)^2}{2\int_0^T {x_1}^2dt\int_0^T {\dot{x}_1}^2dt-(\int_0^T x_1\dot{x}_1dt)^2}\end{aligned} \tag{12}$$

By replacing the period parameter T with Φ/ω_{1e} (i.e., $T = \Phi/\omega_{1e}$), (12) can be rewritten as

$$\begin{aligned}\gamma &= 2\zeta_1\omega_1\frac{\int_0^\Phi x_1\dot{x}_1d\varphi}{\int_0^\Phi {x_1}^2d\varphi}\frac{\int_0^\Phi {x_1}^2d\varphi\int_0^\Phi {\dot{x}_1}^2d\varphi}{2\int_0^\Phi {x_1}^2d\varphi\int_0^\Phi {\dot{x}_1}^2d\varphi-(\int_0^\Phi x_1\dot{x}_1d\varphi)^2}\\ \lambda &= \frac{(\int_0^\Phi x_1\dot{x}_1d\varphi)^2}{2\int_0^\Phi {x_1}^2d\varphi\int_0^\Phi {\dot{x}_1}^2d\varphi-(\int_0^\Phi x_1\dot{x}_1d\varphi)^2}\end{aligned} \tag{13}$$

Further, the structure response corresponds to the approximate un-damped SDOF system (given in (8)) can be expressed by a general equation, given as

$$x_1 = a\cos(\omega_{1e}t+\varphi_0) \tag{14}$$

where a is the amplitude and φ_0 is a phase angle.

Substituting (14) into (13) and using the definition of ${\omega_{1e}}^2 = \gamma + {\omega_1}^2$ leads to a quadratic equation of the equivalent natural frequency ω_{1e}, given as

$${\omega_{1e}}^2 + \frac{2(1-\cos(2\Phi))(2\Phi-\sin(2\Phi))}{8\Phi^2-2\sin^2(2\Phi)-(1-\cos(2\Phi))^2}\zeta_1\omega_1\omega_{1e} - {\omega_1}^2 = 0 \tag{15}$$

Thus, the natural frequency ω_{1e} of the approximate un-damped SDOF system, as shown in Figure 2, can be obtained, given by

$$\begin{aligned}\omega_{1e} &= \omega_1 coe\\ coe &= \sqrt{1+\left[\frac{(1-\cos(2\Phi))(2\Phi-\sin(2\Phi))}{8\Phi^2-2\sin^2(2\Phi)-(1-\cos(2\Phi))^2}\right]^2{\zeta_1}^2}-\frac{(1-\cos(2\Phi))(2\Phi-\sin(2\Phi))}{8\Phi^2-2\sin^2(2\Phi)-(1-\cos(2\Phi))^2}\zeta_1\end{aligned} \tag{16}$$

where *coe* is defined as a frequency ratio of the approximate un-damped SDOF system to the primary damped one. It is important to point out that the equivalent natural frequency ω_{1e} given in (16) is closely related to the damping ratio ζ_1 of the primary damped SDOF system implying the structural damping contribution. In addition, *coe* is also nonlinearity dependent on the period parameter Φ. It has been demonstrated that $\Phi = \pi/2$ can provide a satisfactory result for the damper optimal design. For more information regarding this period parameter, readers can refer to the previous investigations [42–45].

3.2. H_2 Norm Optimization

Similar to (5), a few parameters for the approximate un-damped SDOF system are introduced, including the frequency ratio $\overline{\beta}$ and the damping ratio $\overline{\zeta}_2$. Two more non-dimensional parameters, i.e., the external excitation frequency $\overline{\phi}$ and the time parameter $\overline{\tau}$ are also included, defined as

$$\overline{\beta} = \frac{\omega_2}{\omega_{1e}},\ \overline{\zeta}_2 = \frac{c_2}{2m_2\omega_{1e}},\ \overline{\phi} = \frac{\omega}{\omega_{1e}},\ \overline{\tau} = \omega_{1e}t \tag{17}$$

They are connected to the parameters of the primary damped SDOF system, given in (5) through the following relations:

$$\beta = \overline{\beta} coe,\ \zeta_2 = \overline{\zeta}_2 coe,\ \phi = \overline{\phi} coe,\ \tau = \frac{\overline{\tau}}{coe} \tag{18}$$

Thus, the EOMs for the primary analogue TLIMD-SDOF system with the damped SDOF system represented by an approximate un-damped one, i.e., the approximate TLIMD-SDOF system, can be written as

$$\begin{array}{l} \ddot{z}_1 + z_1 + \mu\overline{\beta}^2(z_1 - z_2) + 2\overline{\zeta}_2\mu\overline{\beta}(\dot{z}_1 - \dot{z}_2) = -e^{i\overline{\phi}\overline{\tau}} \\ [{\alpha_1}^2 + \frac{1}{3}u_{32}(1 - \alpha_2 + {\alpha_2}^2)]\ddot{z}_2 + \overline{\beta}^2(z_2 - z_1) + 2\overline{\zeta}_2\overline{\beta}(\dot{z}_2 - \dot{z}_1) = \alpha_1 e^{i\overline{\phi}\overline{\tau}} + \frac{1}{2}u_{32}(\alpha_2 - 1)e^{i\overline{\phi}\overline{\tau}} \end{array} \tag{19}$$

Note that (19) and (6) possess a unified expression, i.e., (19) can be directly obtained from (6) by ignoring the structural damping $\zeta_1 = 0$ with substitutions of the frequency ratio $\beta = \overline{\beta}$, the damping ratio $\zeta_2 = \overline{\zeta}_2$, the excitation frequency $\phi = \overline{\phi}$ and the time parameter $\tau = \overline{\tau}$.

The structural responses in (19) can be expressed as

$$z_1 = z_{1m}e^{i\overline{\phi}\overline{\tau}},\ z_2 = z_{2m}e^{i\overline{\phi}\overline{\tau}} \tag{20}$$

By inserting (20) into (19), the complex amplitudes for the host structure z_{1m} and the lever z_{2m} can be obtained, given as

$$z_{1m} = \frac{A_1 + B_1\overline{\zeta}_2 i}{C + D\overline{\zeta}_{22} i},\ z_{2m} = \frac{A_2 + B_2\overline{\zeta}_2 i}{C + D\overline{\zeta}_{22} i} \tag{21}$$

where

$$\begin{array}{l} A_1 = \overline{\beta}^2(1 - \mu\mu_2) - \mu_1\overline{\phi}^2,\ B_1 = 2\overline{\beta}\overline{\phi}(1 - \mu\mu_2) \\ A_2 = \mu_2\left(\overline{\phi}^2 - 1\right) + \overline{\beta}^2(1 - \mu\mu_2),\ B_2 = 2\overline{\beta}\overline{\phi}(1 - \mu\mu_2) \\ C = \mu_1\overline{\phi}^2\left(1 - \overline{\phi}^2 + \overline{\beta}^2\mu\right) - \overline{\beta}^2\left(1 - \overline{\phi}^2\right),\ D = 2\overline{\beta}\overline{\phi}\left(\overline{\phi}^2 + \mu\mu_1\overline{\phi}^2 - 1\right) \\ \mu_1 = {\alpha_1}^2 + \frac{1}{3}u_{32}(1 - \alpha_2 + {\alpha_2}^2),\ \mu_2 = \alpha_1 + \frac{1}{2}u_{32}(\alpha_2 - 1) \end{array} \tag{22}$$

For the white noise external excitation with a constant spectral density S_0 applied on the host structure, the variance of the host structure response can be obtained from the integral operation:

$$\sigma_{z_1}^2 = \int_{-\infty}^{+\infty} |z_{1\mathrm{m}}|^2 S_0 d\omega = S_0\omega_1 \int_{-\infty}^{+\infty} |z_{1\mathrm{m}}|^2 d\phi \tag{23}$$

The performance index is defined by

$$I_H = \frac{\sigma_{z_1}^2}{2\pi} = \frac{1}{2\pi}\int_{-\infty}^{+\infty} |z_{1m}|^2 d\phi \tag{24}$$

where the integral part inside (24) can be calculated by

$$\int_{-\infty}^{+\infty} |z_{1\mathrm{m}}|^2 d\phi = \int_{-\infty}^{+\infty} \frac{\psi(\phi)}{\Gamma(\phi)\Gamma^*(\phi)} d\phi = \frac{\pi}{a_4}\frac{\mathrm{Det}[G]}{\mathrm{Det}[F]} \tag{25}$$

where

$$\begin{aligned}
&\psi(\phi) = b_3\phi^6 + b_2\phi^4 + b_1\phi^2 + b_0\\
&\Gamma(\phi) = a_4(i\phi)^4 + a_3(i\phi)^3 + a_2(i\phi)^2 + a_1(i\phi) + a_0\\
&\mathbf{G} = \begin{bmatrix} b_3 & b_2 & b_1 & b_0 \\ -a_4 & a_2 & -a_0 & 0 \\ 0 & -a_3 & a_1 & 0 \\ 0 & a_4 & -a_2 & a_0 \end{bmatrix},\ \mathbf{F} = \begin{bmatrix} a_3 & -a_1 & 0 & 0 \\ -a_4 & a_2 & -a_0 & 0 \\ 0 & -a_3 & a_1 & 0 \\ 0 & a_4 & -a_2 & a_0 \end{bmatrix}\\
&b_0 = \overline{\beta}^4(\mu\mu_2 - 1)^2,\ b_1 = 2\overline{\beta}^2(\mu\mu_2 - 1)\left(\mu_1 - 2\overline{\zeta}_2{}^2 + 2\mu\mu_2\overline{\zeta}_2{}^2\right),\ b_2 = \mu_1{}^2,\ b_3 = 0\\
&a_0 = -\overline{\beta}^2,\ a_1 = -2\overline{\beta}\overline{\zeta}_2,\ a_2 = -\mu_1 - \overline{\beta}^2 - \overline{\beta}^2\mu\mu_1,\ a_3 = -2\overline{\beta}\overline{\zeta}_2(\mu\mu_1 + 1),\ a_4 = -\mu_1
\end{aligned} \tag{26}$$

Then, the optimal frequency ratio $\overline{\beta}$ and the damping ratio $\overline{\zeta}_2$ can be determined by the following equations:

$$\frac{\partial I_H}{\partial \overline{\beta}} = 0,\ \frac{\partial I_H}{\partial \overline{\zeta}_2} = 0 \tag{27}$$

with the solutions given by

$$\begin{aligned}
\overline{\beta}_{opt} &= \frac{1}{\mu\mu_1+1}\sqrt{\frac{\mu_1(\mu_1\mu_2\mu^2+\mu_1\mu+2)}{2(1-\mu\mu_2)}}\\
\overline{\zeta}_{2,opt} &= \frac{\mu_1}{2}\sqrt{\frac{\mu(\mu_1\mu_2\mu^2+3\mu_1\mu+4)}{2(\mu\mu_1+1)(\mu_1\mu_2\mu^2+\mu_1\mu+2)}}
\end{aligned} \tag{28}$$

Note that the proposed solution (28) for the TLIMD optimal parameters is held as long as the condition $\alpha_1 < \frac{1}{\mu} - \frac{1}{2}\mu_{32}(\alpha_2 - 1),\ (\alpha_1 \le \alpha_2)$ is fulfilled [22].

The performance index under the optimal tuning condition can be calculated, given as

$$I_{H,opt} = \frac{\mu_1(1-\mu\mu_2)\left(\mu^4\mu_1{}^2\mu_2{}^2 + 4\mu^3\mu_1{}^2\mu_2 + 3\mu^2\mu_1{}^2 + 6\mu^2\mu_1\mu_2 + 10\mu\mu_1 + 8\right)}{4\sqrt{2}(\mu\mu_1+1)^2\overline{\beta}_{opt}(\mu_1\mu_2\mu^2+\mu_1\mu+2)\overline{\zeta}_{2.opt}} \tag{29}$$

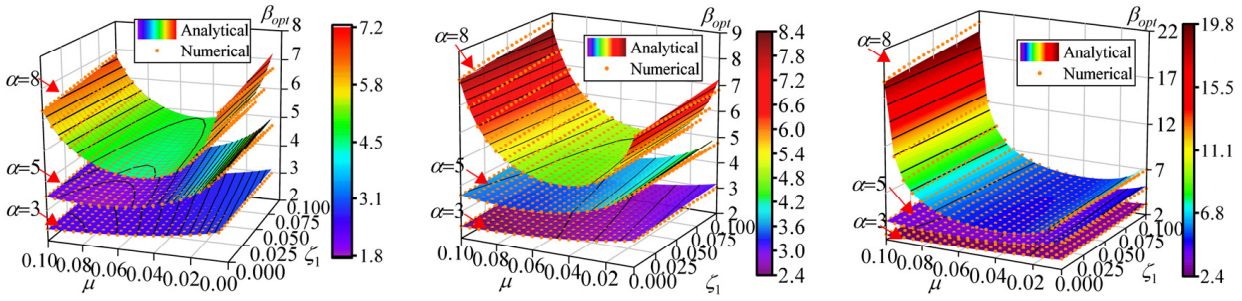
Equation (18) connections the parameters defined in the approximate TLIMD-SDOF system and the one defined in the primary analogue TLIMD-SDOF system. Thus, the optimal parameters given by (28) can be transferred to

$$\beta_{opt} = \overline{\beta}_{opt}coe,\ \zeta_{2,opt} = \overline{\zeta}_{2,opt}coe \tag{30}$$

which provides more intuitive formulae for the TLIMD optimal design. Furthermore, it should be emphasized that the proposed formulae for the TLIMD optimal design (given in (30)) explicitly indicate the contribution from the structural inherent damping ζ_1, since *coe* is a function of the structural damping, cf. (16).

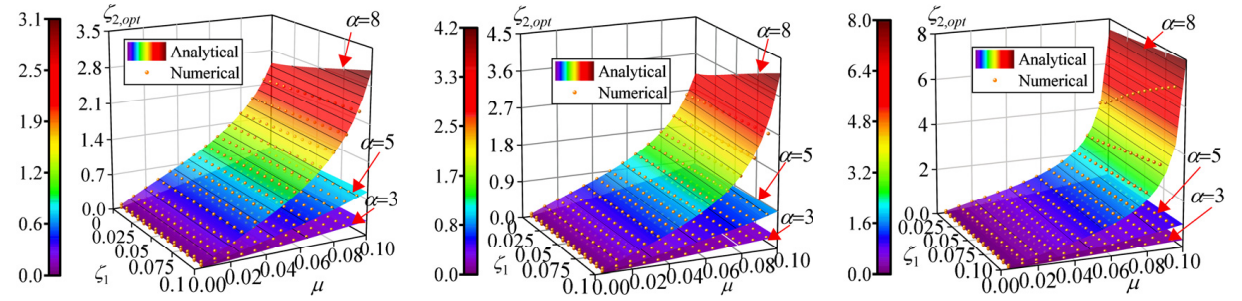
4. Optimal Formulae Validation

Section 3 develops a theoretical calibration framework for the TLIMD optimization, in which a set of closed-form formulae for the TLIMD optimal parameters are developed based on the classic H_2 norm optimization criterion. Benefiting from Anh's dual-equivalent linearization method, the structural damping influence is also included in the damper design process. The proposed Formula (30) (determined by the H_2 optimization criterion and indicated by the word Analytical in Figures 3–5) for the TLIMD optimal parameters are validated by the comparison with the results obtained through the numerical optimization technique (here using the particle swarm optimization, indicated by the word Numerical in Figures 3–5). A uniform length ratio is assumed to be $\alpha_1 = \alpha_2 = \alpha$ given the practical consideration.



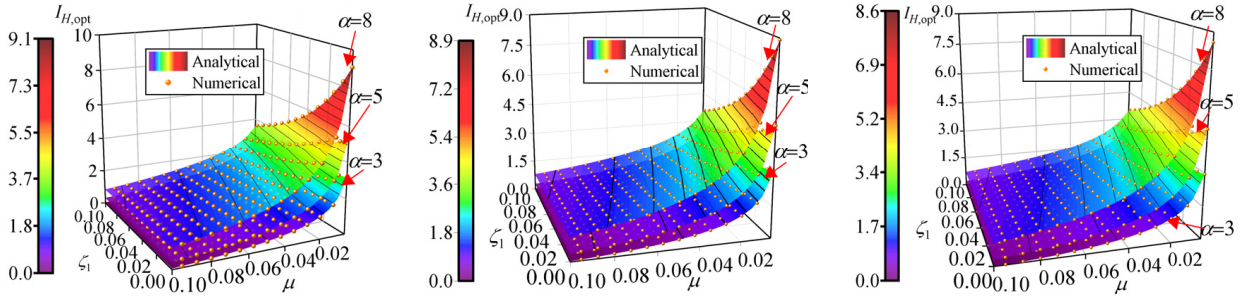
(**a**) μ_{32} = 0.05 (**b**) μ_{32} = 0.2 (**c**) μ_{32} = 0.5

Figure 3. The optimal frequency ratio β_{opt} obtained by the proposed Formula (30) (denoted by Analytical) and by the numerical optimization technique (denoted by Numerical) under the combination of various mass ratio μ, lever mass ratio μ_{32} (0.05, 0.2 and 0.5), damping ratio ζ_1 and length ratio α (3, 5 and 8).



(**a**) μ_{32} = 0.05 (**b**) μ_{32} = 0.2 (**c**) μ_{32} = 0.5

Figure 4. The optimal damping ratio $\zeta_{2,\mathrm{opt}}$ obtained by the proposed Formula (30) (denoted by Analytical) and by the numerical optimization technique (denoted by Numerical) under the combination of various mass ratio μ, lever mass ratio μ_{32} (0.05, 0.2 and 0.5), damping ratio ζ_1 and length ratio α (3, 5 and 8).



(**a**) μ_{32} = 0.05 (**b**) μ_{32} = 0.2 (**c**) μ_{32} = 0.5

Figure 5. The optimal performance indices $I_{H,opt}$ obtained by the proposed Formula (29) (denoted by Analytical) and by the numerical optimization technique (denoted by Numerical) under the combination of various mass ratio μ, lever mass ratio μ_{32} (0.05, 0.2 and 0.5), damping ratio ζ_1 and length ratio α (3, 5 and 8).

Figure 3 compares the optimal frequency ratio β_{opt} determined by the proposed formula (30) and the one obtained by the numerical optimization technique (here using the particle swarm optimization). As seen, the optimal values calculated by (30) show good agreement with the one determined by the numerical technique under all the selected cases. Even though, a large length ratio (such α = 8) and structural damping ratio

(ζ_1 = 0.1) may increase their discrepancy, the relative difference is still less than 5%. In addition, the β_{opt} tends to increase with the mass ratio μ and damping ratio ζ_1 under a small length ratio condition (such α = 3), while it shows nonlinear variation tendency when adopting a relatively large length ratio (such α = 8). β_{opt} shows monotonous variation tendency with the length ratio α, and its values are all larger than 1.

Figure 4 implies that the optimal damping ratio obtained from the two approaches provides almost identical results only under the small mass ratio μ condition. When assigning a large mass ratio, for instance $\mu > 0.08$, the difference between the analytically determined results and the numerically determined one is around 96%. In addition, a large mass ratio μ and length ratio α normally calls for a large optimal damping ratio $\zeta_{2,opt}$. The performance indices under the two optimal tuning configurations are given in Figure 5. The results further confirm the priority of the proposed formulae, which provide a consistent conclusion with the numerically optimized one.

5. Control Performance Evaluation

The ground motion-excited (by the white noise and the earthquake excitation, respectively) TLIMD-structure responses are evaluated in the current section. Here, a uniform length ratio is also assumed to be $\alpha_1 = \alpha_2 = \alpha$ (i.e., $l_2 = l_3$) given the practical consideration. Previous studies indicate that the lever can be treated as an ideal inerter element under a certain structural configuration [22]. Thus, for comparison, two of the most classic inerter-based dampers (shown in Figure 6), i.e., the tuned inerter damper (TID) and the tuned mass damper inerter (TMDI), are included in the current discussion. b denotes the inertance of the inerter (i.e., the apparent mass). A detailed definition of b can be found in the cited references [1–3]. The inertance ratio is defined as $\mu_b = b/m_1$. The lever mass is ignored in the following discussion $\mu_{32} = 0$ given its minor influence in a practical application. For a fair comparison, the effective mass of these three dampers are unified, i.e., $(m_2 + b)_{\text{TMDI}} = (b)_{\text{TID}} = (m_2\alpha^2)_{\text{TLIMD}}$.

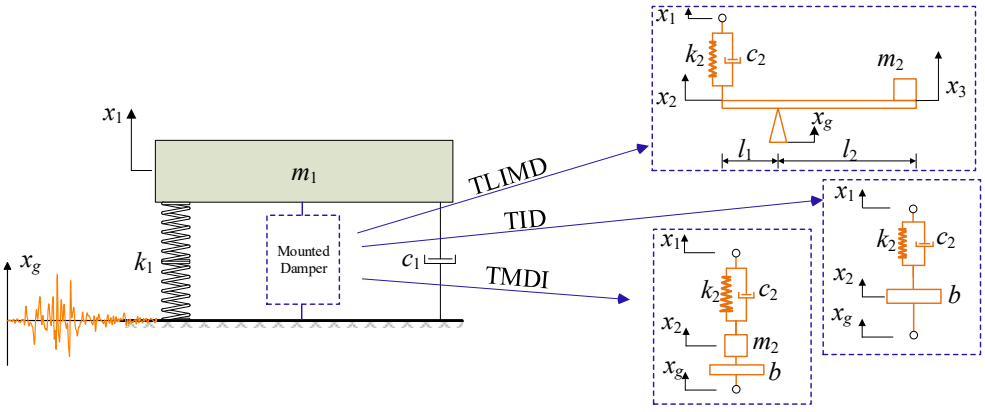


Figure 6. Schematic configurations of these three dampers.

5.1. White Noise-Excited Structure Responses

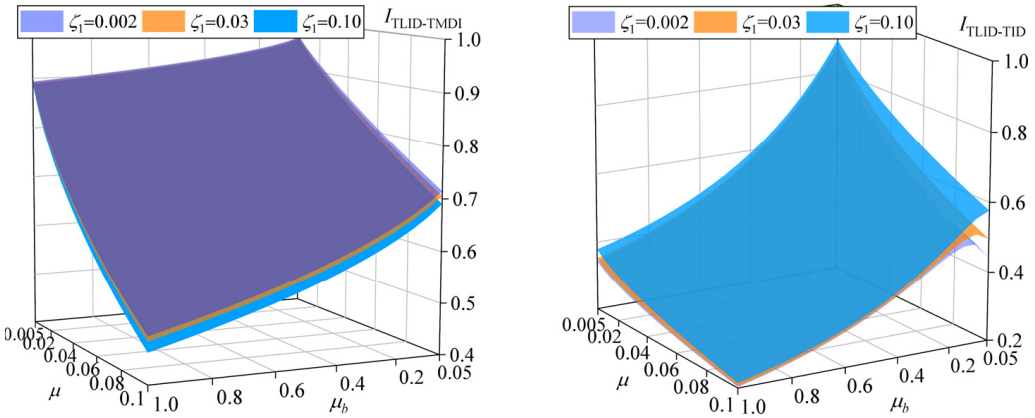
The control performance of the TLIMD compared with TID and TMDI are quantified by the following two indices, defined as

$$I_{\text{TLIMD-TMDI}} = \frac{I_{H\text{-TLIMD}}}{I_{H\text{-TMDI}}},\ I_{\text{TLIMD-TID}} = \frac{I_{H\text{-TLIMD}}}{I_{H\text{-TID}}} \tag{31}$$

where $I_{H\text{-TLIMD}}$, $I_{H\text{-TMDI}}$ and $I_{H\text{-TID}}$ represent the variance of the TLIMD, TMDI or TID equipped with host structure responses, respectively. According to the definition, the TLIMD is considered to be a better perform than other dampers when $I_{\text{TLIMD-TMDI}}$ or $I_{\text{TLIMD-TID}}$ is less than 1.

Figure 7 shows the variation tendency of the two performance indices (given in (31)) with various critical parameters. The concentrated mass m_2 used in TLIMD and TMDI

are set to the same, with its value varying from 0.005 to 0.1, i.e., μ = 0.005~0.1. The inertance ratio μ_b of TMID and TID are identical, taken as μ_b = 0.05~1.0, and the length ratio $\alpha_1 = \sqrt{1+\mu_b/\mu}$ can be determined from the equilibrium $(m_2+b)_{\text{TMDI}} = (m_2\alpha^2)_{\text{TLIMD}}$. The optimal parameters for the TLIMD are determined by (30), while the TMDI and TID are optimized by numerical technique. As seen, both indices are below 1 under the selected configuration cases, which exhibits the superiority of the TLIMD. As expected, the increases in mass ratio μ and inertance ratio μ_b are always beneficial to the TLIMD control performance. The enhancement of the structural mass ratio ζ_1 leads to a decrease of $I_{TLIMD\text{-}TMDI}$, while inducing an increase in $I_{\text{TLIMD-TID}}$. Nevertheless, the TLIMD still shows big advantages over those conventional devices, even under the larger structural damping scenario (such as ζ_1 = 10%).



(**a**) $I_{TLIMD\text{-}TMDI}$ (**b**) $I_{TLIMD\text{-}TID}$

Figure 7. TLIMD performance indices variation tendency.

Figure 8 further evaluates the TLIMD control performance in terms of the frequency response function (FRF) of the host structure. As seen, the TMDI and TID provide almost identical result, while the TLIMD (indicated by the red dashed line) results in a smaller structure response. Thus, it is concluded that the TLIMD consistently outperforms the TMDI and TID in terms of the structural peak response when adopting the H_2 calibration criterion.

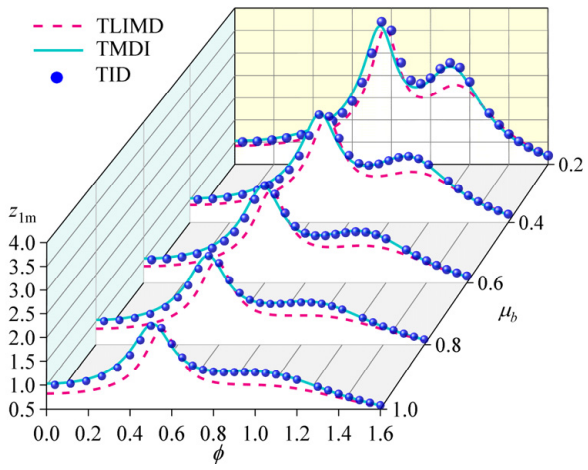


Figure 8. Frequency response function (FRF) of the host structure equipped with different kinds of dampers.

5.2. Sensitivity Analysis Under Detuning Situations

In practical application, the target optimal parameters for the TLIMD may be deviated from the optimization due to the manufacture errors of device, ageing of the spring and damper, and frequency change in the primary structure in service, directly resulting in the detuning of the TLIMD and deteriorating the control performance. Hence, the sensitivity analysis is essential to estimate the performance of the TLID once the detuning occurs.

Previous studies, in general, assume that the frequency and damping ratios of the damper device are varied in a range normalized to the optimal values to obtain the ratio of these maximum amplitudes of the primary structure to the optimized values using a widely used tool contour plot. However, an issue may arise: the comparison of the sensitive performance between different kinds of dampers is difficult if they have a similar sensitivity. Additionally, one contour plot only represents the one specified mass ratio or inertance mass ratio. It cannot roundly evaluate which kind of damper is insensitive to parameters variation, and a new index needs to be introduced. Therefore, the above question is discussed in this subsection through the sensitivity comparisons among TID-, TMDI- and TLIMD-controlled systems. The current discussion is focused on two critical parameters, i.e., the frequency ratio β and the damping ratio ζ_2, where their deviation value in TLIMD/TMDI/TID are set to $\beta = (0.8\sim1.2)\beta_{opt}$ and $\zeta_2 = (0.8\sim1.2)\zeta_{2,opt}$

Herein, an assessment index called the root mean square error (RMSE) is introduced, defined as

$$RMSE = \sqrt{\sum_{i=1}^{M}\sum_{j=1}^{N}\frac{\left[I_{i,j}(\beta,\zeta_2) - I_{H,opt}(\beta_{opt},\zeta_{2,opt})\right]^2}{MN}} \tag{32}$$

where M and N represent the sum of deviation points for frequency and damping ratios, respectively and i and j are the number of M and N.

Figure 9 shows the RMSE value versus the mass ratio μ. It can be observed that the TLIMD exhibits the minimal value for all the selected cases, especially under the large mass ratio condition (such as $\mu = 0.1$). Furthermore, the increase in mass ratio μ and the inertance ratio μ_b can diminish the RMSE of all these dampers, and thus somehow enhance the robustness of the damper performance.

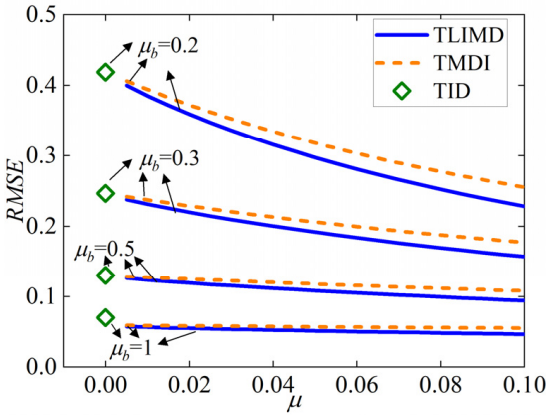


Figure 9. The RMSE value versus the mass ratio.

Figure 10 shows the maximum amplitude ratios of primary structure with various frequency and damping ratios deviated from the damper optimal design values. The mass ratio μ for the TLIMD and TMDI is set to 0.01, and the inertance ratio for the TMDI and TID is set to 0.1. It can be seen that the contour lines for the TMDI and TID looks the same while the sensitive performance of the TLIMD may be better than the others due to its small value. Figure 10d further ensures this conclusion, in which the TLIMD provides the minimal indices I_H value.

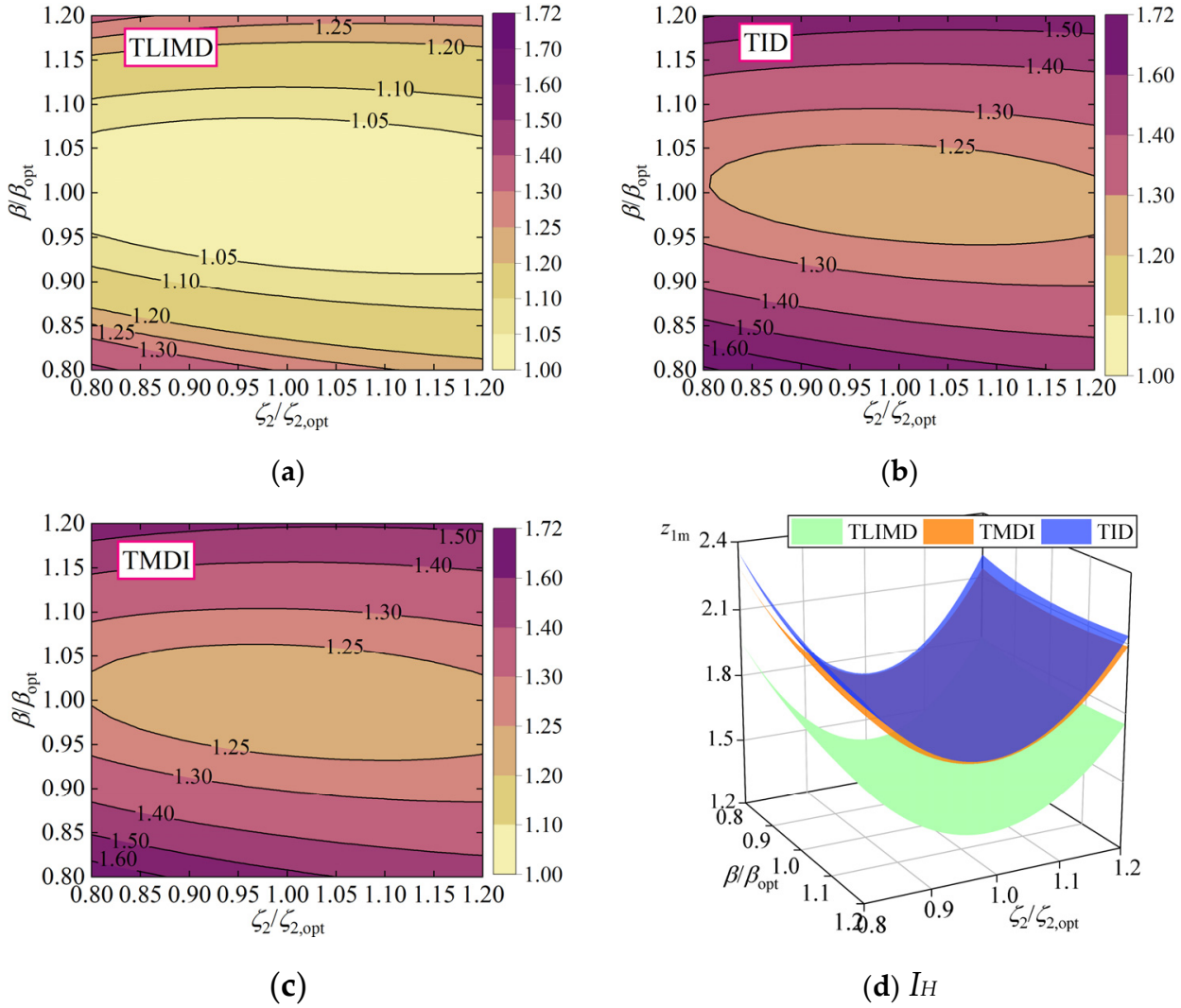
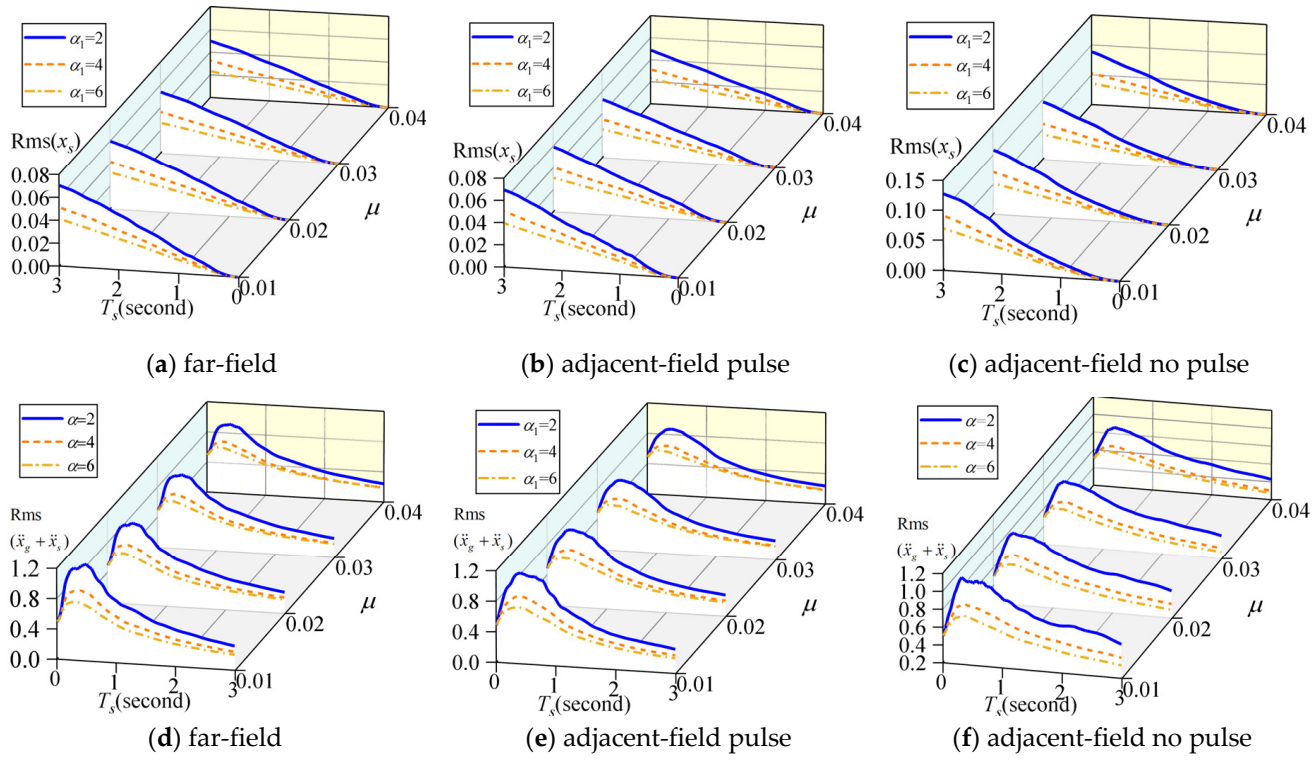


Figure 10. Maximum amplitude ratios of primary structure between deviations and optimization for (**a**) TLID, (**b**) TID and (**c**) TMDI, and (**d**) a 3D plot for maximum amplitude comparison between them.

5.3. Seismic-Induced Vibration

According to the guideline of FEMA P-695 [46], 44 far-field, 28 near-field pulse and 28 no-pulse ground motion records are investigated here, and the peak acceleration is all set to 0.3 g. Statistical results of the structure responses are given in Figures 11 and 12. Figure 11 shows the root mean square (RMS) of the structure relative displacement x_1 and absolute acceleration responses $\ddot{x}_g + \ddot{x}_1$. As seen, the structural responses can be effectively attenuated by increasing the length ratio α and the mass ratio μ under all types of ground motion excitation. A comparison case for these three dampers is given in Figure 12, where the length ratio α and the mass ratio μ are set to $\mu = 0.02$ and $\alpha = 3$. As seen, the TLIMD consistently provides the minimal values.

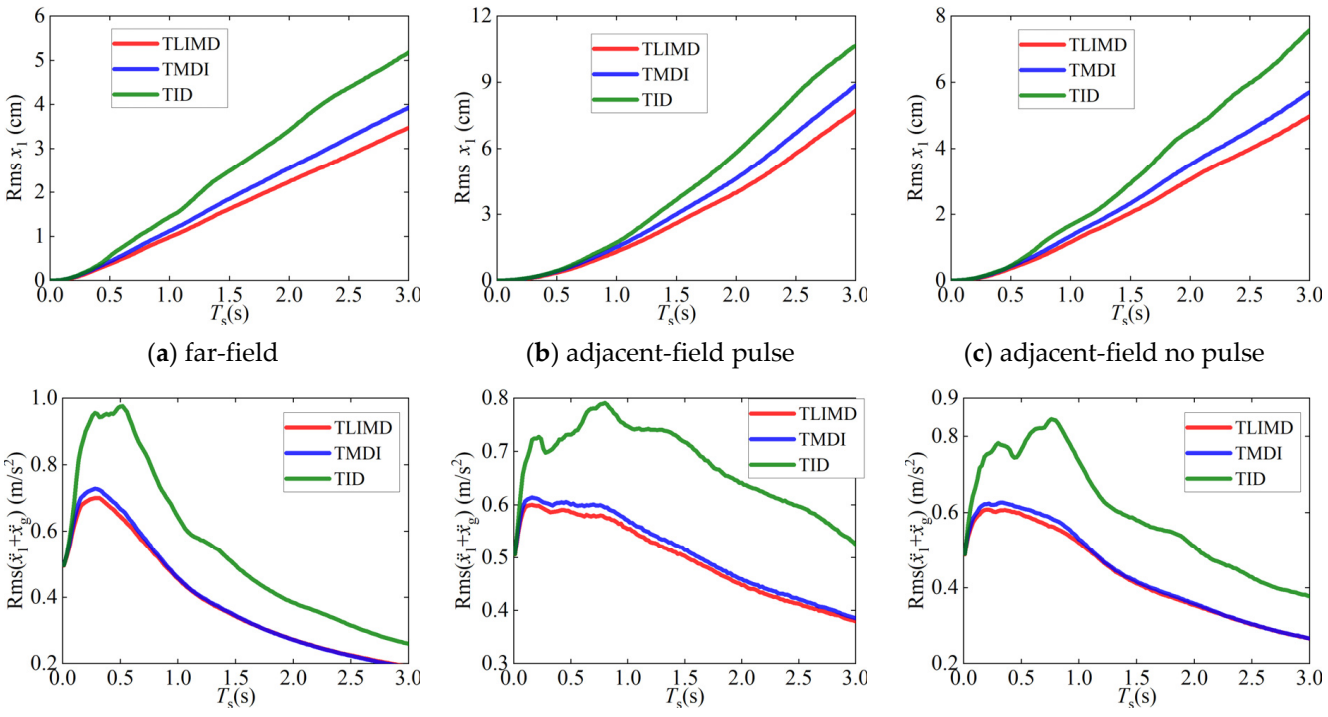
Here, three typical ground motions, given in Figure 13, is selected in the following discussion, and two types of structures (i.e., the long and short period structures, $T_s = 0.5$ and 2 s) are considered. For both the short (given in Figure 14) and long period (given in Figure 15) structures, the TLIMD exhibits a noticeably better control performance than the TID. However, for the long period structure under the adjacent-field pulse ground motion, the TLIMD is not significantly better than the TMDI, as demonstrated in Figure 15c,f.



(**a**) far-field (**b**) adjacent-field pulse (**c**) adjacent-field no pulse

(**d**) far-field (**e**) adjacent-field pulse (**f**) adjacent-field no pulse

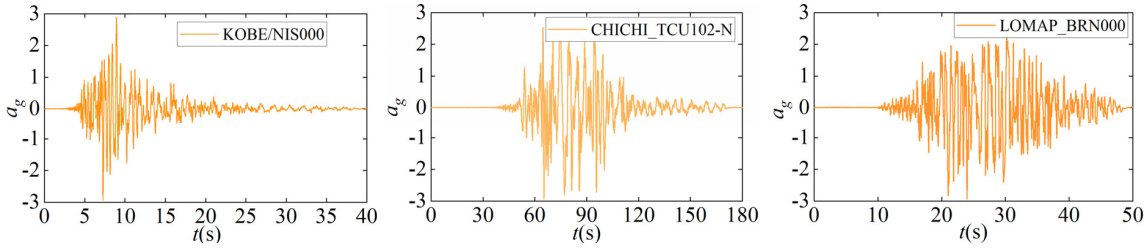
Figure 11. Root mean square (RMS) value of the TLIMD equipped structure (**a**–**c**) relative displacement and (**d**–**f**) absolute acceleration responses. T_s is the natural period of the host structure.



(**a**) far-field (**b**) adjacent-field pulse (**c**) adjacent-field no pulse

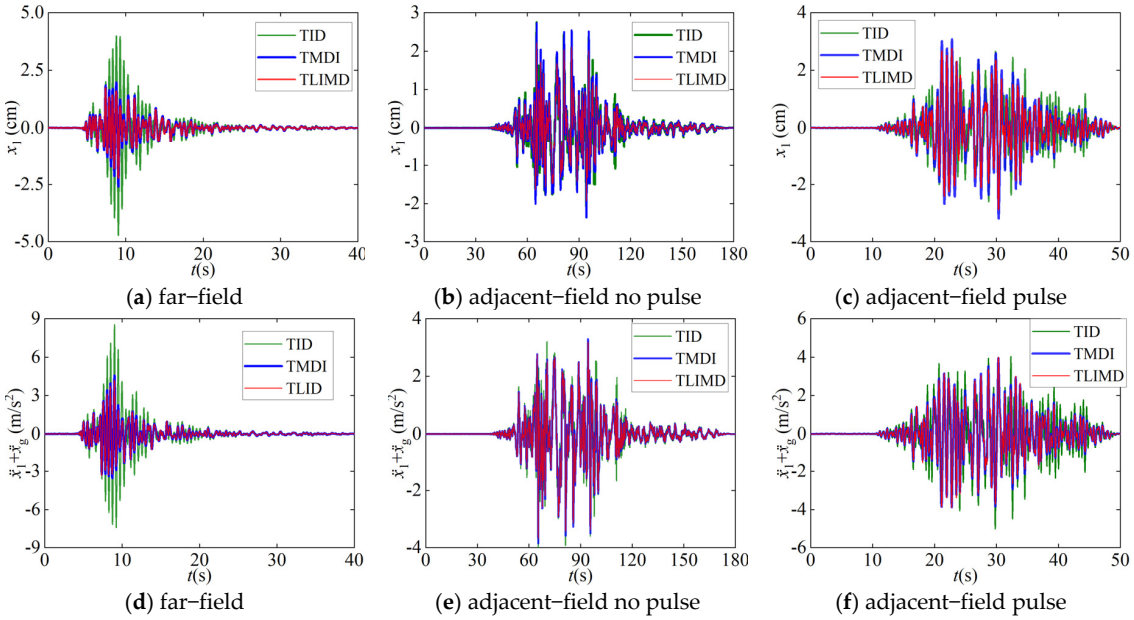
(**d**) far-field (**e**) adjacent-field pulse (**f**) adjacent-field no pulse

Figure 12. Root mean square (RMS) value of the damper equipped structure (**a**–**c**) relative displacement and (**d**–**f**) absolute acceleration responses, with μ = 0.02 and α = 3.



(**a**) far−field (**b**) adjacent−field no pulse (**c**) adjacent−field pulse

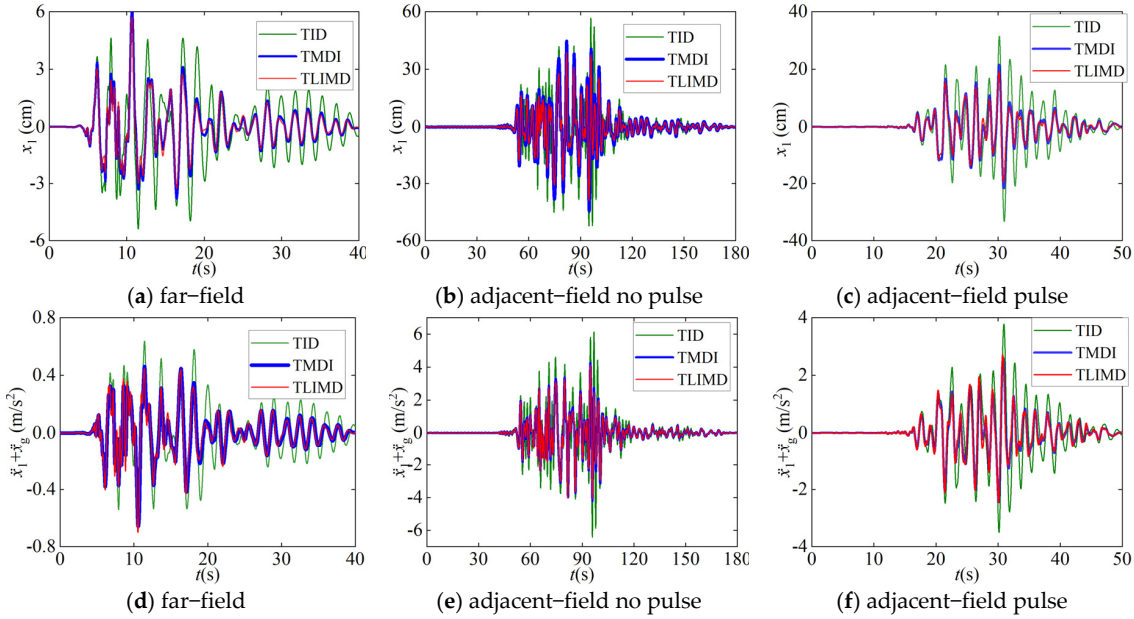
Figure 13. Three typical ground motion acceleration records.



(**a**) far−field (**b**) adjacent−field no pulse (**c**) adjacent−field pulse

(**d**) far−field (**e**) adjacent−field no pulse (**f**) adjacent−field pulse

Figure 14. The damper equipped short period (T_s = 0.5) structure (**a**–**c**) relative displacement and (**d**–**f**) absolute acceleration responses.



(**a**) far−field (**b**) adjacent−field no pulse (**c**) adjacent−field pulse

(**d**) far−field (**e**) adjacent−field no pulse (**f**) adjacent−field pulse

Figure 15. The damper equipped short period (T_s = 2) structure (**a**–**c**) relative displacement and (**d**–**f**) absolute acceleration responses.

6. Conclusions

The present study develops theoretical calibration framework for a novel tuned lever inerter-like mass damper (TLIMD) optimization. The host structure inherent damping is explicitly included in the calibration process, thus leading to generalized formulae for the TLIMD's optimal parameters. Owing to the inertial amplification property (of the lever) and the geometric configuration advantage, the optimized TLIMD exhibits better performance than the classic inerter-based dampers (e.g., the TMDI and TID). The main conclusions are as follows.

In terms of the vibration control performance, three main advantages are summarized for the optimized TLIMD (by the proposed formulae). Firstly, comparing to the traditional inerter-based damper (e.g., the TID and TMDI), the TLIMD can significantly attenuate the variance of structure displacement, especially under the large mass ratio and lever length ratio (known as the inertia amplification ratio) condition. Secondly, with the introduction of the host structure damping (even at a high damping ratio value such as ζ_1 = 10%), the TLIMD still exhibits significant advantages over the TMDI and TID. Finally, under the same frequency and damping ratio detuning condition (the robustness analysis), the TLIMD not only yields smaller root mean square error (RMSE) values but also results in a relatively smaller displacement RMS value of the main structure compared to the TID and TMDI. Even though the control performance of the TLIMD is not remarkable compared with the TMDI under some special cases, it is still considered a cost-effective solution in real application.

Author Contributions: K.X.: Conceptualization, Methodology, Investigation, Software, Writing—original draft, Writing—review and editing. W.W.: Methodology, Software, Writing—review and editing. H.L.: Conceptualization, Investigation, Software. A.L.: Software, Investigation. J.G.: Investigation, Software. J.Y.: Conceptualization, Supervision. B.C.: Conceptualization, Investigation, Writing—review and editing, Supervision. All authors have read and agreed to the published version of the manuscript.

Funding: This research was funded by the National Natural Science Foundation of China (No. 52378507), the Hunan Provincial Ten Key Technological Projects (No. 2023GK1030), the Hunan Provincial Natural Science Foundation of China (No. 2023JJ30129), Young Talent Fund of Association for Science and Technology in Shaanxi, China (No. 20240432; No. 20240419) and Shaanxi Province Science and Technology Activities for Overseas Students Selected Funding Project (No. 2023-007).

Institutional Review Board Statement: Not applicable.

Informed Consent Statement: Not applicable.

Data Availability Statement: The data presented in this study are available on request from the corresponding author. The data are not publicly available due to privacy.

Conflicts of Interest: The authors declare no conflicts of interest.

References

1. Smith, M.C. Synthesis of mechanical networks: The inerter. *IEEE Trans. Autom. Control* **2002**, *10*, 1648–1662. [CrossRef]
2. Smith, M.C. The inerter: A retrospective. *Annu. Rev. Control Robot. Auton. Syst.* **2020**, *3*, 361–391. [CrossRef]
3. Papageorgiou, C.; Houghton, N.; Smith, M. Experimental testing and analysis of inerter devices. *J. Dyn. Sys. Meas. Control* **2009**, *131*, 011001. [CrossRef]
4. Marian, L.; Giaralis, A. Optimal design of a novel tuned mass-damper-inerter (TMDI) passive vibration control configuration for stochastically support-excited structural systems. *Probab. Eng. Mech.* **2014**, *38*, 156–164. [CrossRef]
5. Giaralis, A.; Taflanidis, A. Optimal tuned mass-damper-inerter (TMDI) design for seismically excited MDOF structures with model uncertainties based on reliability criteria. *Struct. Control Health Monit.* **2018**, *25*, e2082. [CrossRef]
6. Giaralis, A.; Marian, L. Use of inerter devices for weight reduction of tuned mass-dampers for seismic protection of multi-story building: The tuned mass-damper-interter (TMDI). *Act. Passiv. Smart Struct. Integr. Syst.* **2016**, *9799*, 415–424.
7. Lazar, I.; Neild, S.; Wagg, D. Vibration suppression of cables using tuned inerter dampers. *Eng. Struct.* **2016**, *122*, 62–71. [CrossRef]
8. Jangid, R. Optimum tuned inerter damper for base-isolated structures. *J. Vib. Eng. Technol.* **2021**, *9*, 1483–1497. [CrossRef]
9. Gonzalez-Buelga, A.; Lazar, I.; Jiang, J.; Neild, S.; Inman, D. Assessing the effect of nonlinearities on the performance of a tuned inerter damper. *Struct. Control Health Monit.* **2017**, *24*, e1879. [CrossRef]

10. Lu, L.; Xu, J.; Zhou, Y.; Lu, W.; Spencer, B.F. Viscous inertial mass damper (VIMD) for seismic responses control of the coupled adjacent buildings. *Eng. Struct.* **2021**, *233*, 111876. [CrossRef]
11. Garrido, H.; Curadelli, O.; Ambrosini, D. Improvement of tuned mass damper by using rotational inertia through tuned viscous mass damper. *Eng. Struct.* **2013**, *56*, 2149–2153. [CrossRef]
12. Rajana, K.; Wang, Z.; Giaralis, A. Optimal design and assessment of tuned mass damper inerter with nonlinear viscous damper in seismically excited multi-storey buildings. *Bull. Earthq. Eng.* **2023**, *21*, 1509–1539. [CrossRef]
13. Li, C. Evaluation of the lever-type active tuned mass damper for structures. *Struct. Control Health Monit.* **2004**, *11*, 259–271. [CrossRef]
14. Li, C.; Zhou, D. Evaluation of multiple active lever-type tuned mass dampers for structures under ground acceleration. *Eng. Struct.* **2004**, *26*, 303–317. [CrossRef]
15. Gu, M.; Chen, S.; Chang, C. Control of wind-induced vibrations of long-span bridges by semi-active lever-type TMD. *J. Wind Eng. Ind. Aerodyn.* **2002**, *90*, 111–126. [CrossRef]
16. Ma, R.; Bi, K.; Hao, H. Inerter-based structural vibration control: A state-of-the-art review. *Eng. Struct.* **2021**, *243*, 112655. [CrossRef]
17. Wagg, D. A review of the mechanical inerter: Historical context, physical realisations and nonlinear applications. *Nonlinear Dyn.* **2021**, *104*, 13–34. [CrossRef]
18. Smith, M.C. The inerter concept and its application. In Proceedings of the Society of Instrument and Control Engineers (SICE) Annual Conference 2003, Fukui, Japan, 4 August 2003.
19. Deastra, P.; Wagg, D.; Sims, N.D. The realisation of an inerter-based system using fluid inerter. In *Dynamics of Civil Structures, Volume 2, Proceedings of the 36th IMAC, A Conference and Exposition on Structural Dynamics 2018, Orlando, FL, USA, 12–15 February 2018*; Springer: Cham, Switzerland, 2018; pp. 127–134.
20. Li, K.; Gohnert, M. Lever mechanism for vibration isolation. *Appl. Technol. Innov.* **2010**, *1*, 21–28. [CrossRef]
21. Zang, J.; Cao, R.; Zhang, Y. Steady-state response of a viscoelastic beam with asymmetric elastic supports coupled to a lever-type nonlinear energy sink. *Nonlinear Dyn.* **2021**, *105*, 1327–1341. [CrossRef]
22. Xu, K.; Yang, J.M.; Liu, A.F.; Hua, X.G.; Wang, W.X.; Huang, Z.W.; Chen, Z.Q. Tuned Lever Inerter-like Damper. *Mech. Syst. Signal Process.* 2024; *submitted*.
23. Ibrahim, R.A. Recent advances in nonlinear passive vibration isolators. *J. Sound Vib.* **2008**, *314*, 371–452. [CrossRef]
24. Flamnnelly, W.G. Dynamic Anti-Resonance Vibration Isolator. U.S. Patent 3,322,379, 30 May 1967.
25. Liu, C.C.; Jing, X.J.; Li, F.M. Vibration isolation using a hybrid lever-type isolation system with an X-shape supporting structure. *Int. J. Mech. Sci.* **2015**, *98*, 169–177. [CrossRef]
26. Liu, C.C.; Jing, X.J.; Chen, Z.B. Band stop vibration suppression using a passive X-shape structured lever-type isolation system. *Mech. Syst. Signal Process.* **2016**, *69*, 342–353. [CrossRef]
27. Zang, J.; Yuan, T.; Lu, Z.; Zhang, Y.; Ding, H.; Chen, L. A lever-type nonlinear energy sink. *J. Sound Vib.* **2018**, *437*, 119–134. [CrossRef]
28. Yang, K.; Fei, F.; An, H. Investigation of coupled lever-bistable nonlinear energy harvesters for enhancement of inter-well dynamic response. *Nonlinear Dyn.* **2019**, *96*, 2369–2392. [CrossRef]
29. Yilmaz, C.; Kikuchi, N. Analysis and design of passive band-stop filter-type vibration isolators for low-frequency applications. *J. Sound Vib.* **2006**, *291*, 1004–1028. [CrossRef]
30. Yilmaz, C.; Kikuchi, N. Analysis and design of passive low-pass filter-type vibration isolators considering stiffness and mass limitations. *J. Sound Vib.* **2006**, *293*, 171–195. [CrossRef]
31. Yan, B.; Wang, Z.H.; Ma, H.Y.; Bao, H.; Wang, K.; Wu, C. A novel lever-type vibration isolator with eddy current damping. *J. Sound Vib.* **2021**, *494*, 115862. [CrossRef]
32. Yan, B.; Wang, X.J.; Wang, Z.H.; Wu, C.; Zhang, W. Enhanced lever-type vibration isolator via electromagnetic shunt damping. *Int. J. Mech. Sci.* **2022**, *218*, 107070. [CrossRef]
33. Wang, X.J.; Yu, N.; Wu, C.Y.; Zhang, W.; Yan, B. Lever-type high-static-low-dynamicstiffness vibration isolator with electromagnetic shunt damping. *Int. J. Non-Linear Mech.* **2022**, *146*, 104128. [CrossRef]
34. Yan, B.; Yu, N.; Wang, Z.; Wu, C.; Wang, S.; Zhang, W. Lever-type quasi-zero stiffness vibration isolator with magnetic spring. *J. Sound Vib.* **2022**, *527*, 116865. [CrossRef]
35. Li, Z.; Xu, K.; Ma, R.; Bi, K.; Han, Q. A novel lever-arm tuned mass damper inerter (LTMDI) for vibration control of long-span bridges. *Eng. Struct.* **2023**, *293*, 116662. [CrossRef]
36. Gu, M.; Chen, S.; Xiang, H. Buffeting Control of the Yangpu Bridge Using Multiple Tuned Mass Dampers. *J. Vib. Eng. (CN)* **1998**, *1*, 4–11.
37. Lee, E.-T.; Eun, H.-C. Lever-type tuned mass damper for alleviating dynamic responses. *Adv. Civ. Eng.* **2019**, *1*, 1–11. [CrossRef]
38. Li, C.; Xiong, X. Dynamic characteristics of new modeling strategy of lever-type tuned mass damper (LT–TMD). *Build. Sci. Res. Sichuan (CN)* **2003**, *4*, 73–75.
39. Li, C.; Wang, Z. Dynamic characteristics of lever-type multiple tuned mass dampers. *Acta Mech. Solida Sin. (CN)* **2003**, *24*, 011.
40. Li, C.X.; Han, B. Estimating lever-type active multiple tuned mass dampers for structures under harmonic excitation. *J. Mech. Mater. Struct.* **2008**, *3*, 19–43. [CrossRef]

41. Özyar, O.; Yılmaz, Ç. A self-tuning adaptive-passive lever-type vibration isolation system. *J. Sound Vib.* **2021**, *505*, 116159. [CrossRef]
42. Anh, N.D.; Nguyen, N.X. Design of TMD for damped linear structures using the dual criterion of equivalent linearization method. *Int. J. Mech. Sci.* **2013**, *77*, 164–170. [CrossRef]
43. Anh, N.D.; Linh, N.N. A weighted dual criterion of the equivalent linearization method for nonlinear systems subjected to random excitation. *Acta Mech.* **2017**, *229*, 1297–1310. [CrossRef]
44. Anh, N.D.; Nguyen, N.X. Extension of equivalent linearization method to design of TMD for linear damped systems. *Struct. Control Health Monit.* **2011**, *19*, 565–573. [CrossRef]
45. Anh, N.D.; Zakovorotny, V.L.; Hieu, N.N.; Diep, D.V. A dual criterion of stochastic linearization method for multi-degree-of-freedom systems subjected to random excitation. *Acta Mech.* **2012**, *223*, 2667–2684. [CrossRef]
46. Applied Technology Council. *Quantification of Building Seismic Performance Factors*; US Department of Homeland Security, FEMA: Washington, DC, USA, 2009.

Disclaimer/Publisher's Note: The statements, opinions and data contained in all publications are solely those of the individual author(s) and contributor(s) and not of MDPI and/or the editor(s). MDPI and/or the editor(s) disclaim responsibility for any injury to people or property resulting from any ideas, methods, instructions or products referred to in the content.